

Research Article

Stochastic Seismic Analysis and Comparison of Alternative External Dissipative Systems

Laura Gioiella ¹, Enrico Tubaldi,² Fabrizio Gara,³ Luigino Dezi,³ and Andrea Dall'Asta¹

¹*School of Architecture and Design, University of Camerino, Viale della Rimembranza, 63100 Ascoli Piceno, Italy*

²*Department of Civil and Environmental Engineering, University of Strathclyde, 75 Montrose Street, Glasgow G1 1XJ, UK*

³*Department of Civil and Building Engineering and Architecture, Università Politecnica delle Marche, Via Brecce Bianche, Ancona, Italy*

Correspondence should be addressed to Laura Gioiella; laura.gioiella@unicam.it

Received 15 September 2017; Accepted 27 December 2017; Published 29 January 2018

Academic Editor: Ivo Calò

Copyright © 2018 Laura Gioiella et al. This is an open access article distributed under the Creative Commons Attribution License, which permits unrestricted use, distribution, and reproduction in any medium, provided the original work is properly cited.

This paper deals with the seismic retrofit of existing frames by means of external passive dissipative systems. Available in different configurations, these systems allow high flexibility in controlling the structural behaviour and are characterized by some feasibility advantages with respect to dissipative devices installed within existing frames. In particular, this study analyzes and compares the performances of two external solutions using linear viscous dampers. The first is based on the coupling of the building with an external fixed-based steel braced frame by means of dampers placed horizontally at the floor levels. The second is an innovative one, based on coupling the building with a “dissipative tower,” which is a steel braced frame hinged at the foundation level, and activating the dampers through its rocking motion. The effectiveness of the two solutions is evaluated and compared by considering a benchmark existing reinforced concrete building, employing a stochastic dynamic approach, under the assumption of linear elastic behaviour for the seismic performance evaluation. This allows efficiently estimating the statistics of many response parameters of interest for the performance assessment and thus carrying out extensive parametric analyses for different properties of the external systems. The study results provide useful information regarding the design and the relative efficiency of the proposed retrofit solutions.

1. Introduction

Traditional approaches for the seismic performance enhancement and retrofit of buildings by means of passive damping usually involve installing the dissipative devices within the building frame in either diagonal or chevron braces connecting adjacent storeys [1, 2]. This type of damping configuration has been extensively studied in the last decades both experimentally and numerically, with a significant number of works focusing on design criteria and performance assessment [3–11]. However, the use of dampers within building frames presents some disadvantages, especially when employed for the retrofit of existing buildings. The increase of internal actions in the nodes and columns adjacent to the dampers can induce premature local failures [10], strengthening the foundations is generally required, retrofitting operations cause remarkable downtime, and relevant costs must be

sustained. For these reasons, there is an increasing interest on external passive control systems, characterized by minimized interferences with the existing frame, during the installation of the retrofit system and also during the building operation. External damping systems are available in different configurations [11–13], allowing high flexibility in controlling the structural behaviour, but their relative efficiency in terms of seismic performance has not been fully investigated to date. In fact, most of the studies in the literature focus on the most recurrent configuration involving the coupling of the structure to be protected with an external one by means of dampers placed horizontally at the storey level (Figure 1(a)). The external structure can be stiff, or it can be flexible, as in the case of adjacent buildings with different dynamic properties [14–18]. The dampers are activated by the absolute floor displacements in the first case and by the relative floor motion of the systems in the latter one. It is noteworthy that

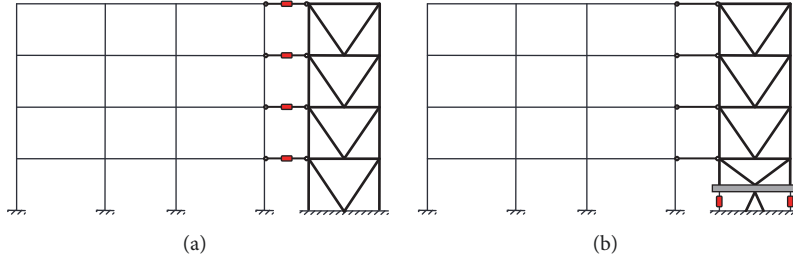


FIGURE 1: Coupling of the existing frame with (a) external fixed-based (FB) structure; (b) rocking-base (RB) tower.

the first configuration can also be designed to achieve mass proportional damping, where the viscous damping constants are proportional to the floor masses [12].

Recently, an innovative external retrofit configuration, denoted as “dissipative tower,” has been proposed. This consists of an external stiff braced structure rigidly linked to the frame at floor levels and connected at the foundations by a hinge (Figure 1(b)). Fluid viscous dampers (FVDs) placed at the base of the external frame and activated by its rocking motion provide energy dissipation to the system, whereas the high stiffness of the braced frame induces a uniform distribution of the interstorey drifts of the protected frame [19].

It is noteworthy that the use of rocking systems has emerged in the last few years as an efficient way to reduce seismic damage [20] and different solutions are available for coupling the frame and the external pinned rocking structures [21, 22]. The rocking tower considered in this study has been employed for the seismic design of new constructions and for retrofitting existing buildings [23, 24] by using a patented technical solution [25]. However, its effectiveness has not been compared yet to the one of more diffused systems involving the coupling between two structures by means of viscous dampers placed horizontally at the floor level.

In this paper, a performance comparison between the two retrofit configurations, that is, the fixed base structure with horizontal FVDs and the rocking tower with vertical FVDs at the base, is carried out through a parametric analysis involving a reference existing building, widely studied in the past [26–28]. The performance comparison is made first in terms of dynamic properties, that is, vibration periods and damping ratios, and then in terms of seismic response of different engineering demand parameters (EDPs) of interest for the safety assessment of the building, the external bracings, and the dampers. In the analyses, the system behaviour is assumed as linear, and the earthquake input is modelled as a stationary stochastic process. Under these assumptions, the problem can be analyzed in the frequency-domain and already available stochastic dynamics techniques [29, 30] can be efficiently used to obtain closed-form expressions of the seismic response statistics, expressed in terms of standard deviation and peak values of the EDPs of interest for a finite time of observation. This approach allows investigating and comparing a wide range of configurations, corresponding to different levels of stiffness and damping of the external systems. The study results give useful information regarding

the design of the external configurations and their relative efficiency for retrofitting existing buildings. It is noteworthy that the elastic behaviour assumption for the problem at hand is reasonable since for practical design applications linear FVDs are often designed in external retrofit systems in such a way as to enhance the performance levels for the building avoiding damages to the structural building components (e.g., immediate occupancy or operational performance level, corresponding to negligible structural damage).

2. Problem Formulation

The reported formulation is suitable for both the two external arrangements; under the assumption of linear elastic behaviour, the equation of motion of the system can be expressed in general as

$$\mathbf{M}\ddot{\mathbf{u}}(t) + \mathbf{C}\dot{\mathbf{u}}(t) + \mathbf{K}\mathbf{u}(t) = \mathbf{M}\mathbf{p}a_g(t), \quad (1)$$

where $\mathbf{u}(t) \in R^l$ is the vector of nodal displacements and rotations; the dot (\cdot) denotes time-derivative; $\mathbf{p} \in R^l$ is the load distribution vector; l denotes the total number of degrees of freedom; and $a_g(t)$ is the external scalar loading function describing the seismic base acceleration. The time constant matrices \mathbf{M} , \mathbf{K} , and \mathbf{C} describe the mass, stiffness, and damping operators $R^l \rightarrow R^l$; they account for the contribution of both the existing frame and the external dissipative bracing system.

Generally, the external bracing system is introduced mainly to control the stiffness and the damping of the system to be protected, while it contributes only marginally to the global mass. In order to give evidence of this aspect in the formulation, it is assumed that the bracing mass is null, and the total displacement vector $\mathbf{u}(t)$ is split into the vector $\mathbf{x}(t) \in R^m$, collecting the active components related to the inertia forces acting on the frame, and the vector $\mathbf{y}(t) \in R^n$ (with $l = m+n$), collecting the other components related to the internal degrees of freedom, including the displacement of the bracing providing the damper deformation. The differential problem is consequently partitioned as follows:

$$\begin{bmatrix} \mathbf{M}_{xx} & \mathbf{0} \\ \mathbf{0} & \mathbf{0} \end{bmatrix} \begin{bmatrix} \ddot{\mathbf{x}} \\ \ddot{\mathbf{y}} \end{bmatrix} + \begin{bmatrix} \mathbf{C}_{xx} & \mathbf{C}_{xy} \\ \mathbf{C}_{yx} & \mathbf{C}_{yy} \end{bmatrix} \begin{bmatrix} \dot{\mathbf{x}} \\ \dot{\mathbf{y}} \end{bmatrix} + \begin{bmatrix} \mathbf{K}_{xx} & \mathbf{K}_{xy} \\ \mathbf{K}_{yx} & \mathbf{K}_{yy} \end{bmatrix} \begin{bmatrix} \mathbf{x} \\ \mathbf{y} \end{bmatrix} = \begin{bmatrix} -\mathbf{M}_{xx}\mathbf{p}_x \\ \mathbf{0} \end{bmatrix} a_g. \quad (2)$$

In the following, the plane problem is considered, by introducing usual simplifications for seismic frame analysis: the floors are assumed to be rigid, only the horizontal component is considered for both the ground motion and the active masses, and these latter are concentrated at the storey levels. In this case, the dimension m of the vector $\mathbf{x}(t)$ coincides with the number of storeys, and additional n degrees of freedom, collected in $\mathbf{y}(t)$, are required to describe the damper deformation.

In the case of the “dissipative rocking tower,” the link between the frame and the bracing at the storey levels is rigid, so $\mathbf{y}(t)$ collects only the vertical displacements related to the rocking motion of the tower at the damper locations. The tower base motion described by $\mathbf{y}(t)$ induces an elastic deformation of the bracing and a set of reactions at the different building floor levels, described by the submatrix \mathbf{K}_{xy} . Similarly, the motion of the building floor results in reactions at the base of the tower, described by the submatrix $\mathbf{K}_{yx} = \mathbf{K}_{xy}^T$. The damper reactions due to the motion of the base of the tower are described by the matrix \mathbf{C}_{yy} .

In the case of the “fixed-based structure,” $\mathbf{y}(t)$ collects the bracing displacements at each floor level, and the damper deformations are induced by the relative motion between the frame and the external structure. In this case, the elastic matrices \mathbf{K}_{yx} and \mathbf{K}_{xy} are null, whereas the elastic response of the bracing is described by \mathbf{K}_{yy} . Both the motions of $\mathbf{x}(t)$ and $\mathbf{y}(t)$ produce damper forces and all the submatrices of \mathbf{C} are different from zero.

Nevertheless, both the retrofit configurations induce non-classical damping because the distribution of the dampers results in a damping matrix which is not proportional to the global mass matrix, nor to the stiffness matrix. The rocking tower corresponds to a highly nonclassically damped system, since the viscous energy dissipation is mainly concentrated at the base of the tower. The second configuration, with the fixed-based bracing, is often characterized by a damping distribution similar to the mass distribution, and it is closer to a classically damped system.

In the following applications, an inherent damping factor equal to 0.05 is also introduced through a Rayleigh damping matrix [31] to provide a realistic description of the response without the added dampers.

2.1. Modal Properties. For the solution of the dynamic problem, corresponding to $a_g(t) = 0$ in (2), a state-space approach is convenient because it gives the opportunity to perform the complex modal analysis of the coupled system, leading to the knowledge of the modal properties in presence of nonclassical damping. For this purpose, it is useful to introduce the vector $\mathbf{v}(t) = \dot{\mathbf{x}}(t)$ and the state vector $\mathbf{z}(t) = [\mathbf{x}(t), \mathbf{v}(t), \mathbf{y}(t)]^T$, collecting the displacements and the velocities of the active displacements and the displacements of the internal nodes. Equation (2) can be reduced to a first-order state space form $\dot{\mathbf{z}}(t) = \mathbf{A}\mathbf{z}(t)$, where the $(2m + n)$ -dimensional state matrix \mathbf{A} is expressed as

$$\mathbf{A} = \begin{bmatrix} \mathbf{0} & \mathbf{I} & \mathbf{0} \\ -\mathbf{M}_{xx}^{-1}(\mathbf{K}_{xx} - \mathbf{C}_{xy}\mathbf{C}_{yy}^{-1}\mathbf{K}_{yx}) & -\mathbf{M}_{xx}^{-1}(\mathbf{C}_{xx} - \mathbf{C}_{xy}\mathbf{C}_{yy}^{-1}\mathbf{C}_{yx}) & -\mathbf{M}_{xx}^{-1}(\mathbf{K}_{xy} - \mathbf{C}_{xy}\mathbf{C}_{yy}^{-1}\mathbf{K}_{yy}) \\ -\mathbf{C}_{yy}^{-1}\mathbf{K}_{yx} & -\mathbf{C}_{yy}^{-1}\mathbf{C}_{yx} & -\mathbf{C}_{yy}^{-1}\mathbf{K}_{yy} \end{bmatrix}. \quad (3)$$

Assuming a solution of the form $\mathbf{z}(t) = \boldsymbol{\varphi}e^{\lambda t}$, the eigenvalue-eigenvector pairs of \mathbf{A} , that is, λ , $\boldsymbol{\varphi}$, are obtained by solving the eigenvalue problem:

$$\mathbf{A}\boldsymbol{\varphi} = \lambda\boldsymbol{\varphi}. \quad (4)$$

In general, a complex eigenvalue has the form

$$\lambda_i = -\xi_i\omega_{0i} + i\omega_{0i}\sqrt{1 - \xi_i^2} \quad (5)$$

and contains information regarding both the damping ratio ξ_i and the corresponding undamped circular frequency ω_{0i} of the i th mode:

$$\begin{aligned} \omega_{0i} &= |\lambda_i| \\ \xi_i &= \frac{-\text{Re}(\lambda_i)}{|\lambda_i|}. \end{aligned} \quad (6)$$

It is noteworthy that the eigenvalues are $(2m + n)$ in total: $2m$ of these are complex conjugates, and the remaining n are real-valued and correspond to the motion of the degrees of freedom with no associated mass.

Closed-form expressions useful for the damper design can be obtained for both the external arrangements by introducing some simplifying assumptions. In the case of coupling with a fixed-based bracing, the dampers can be designed assuming the dampers constants distributed proportionally to the floor masses, that is, the damper constant c_{di} at the i th floor can be expressed as $c_{di} = \alpha M_i$, where α is the proportionality constant and $M_i = [\mathbf{M}_{xx}]_{ii}$ is the floor mass. In the limit case of infinitely stiff contrasting structure, a multi-degree of freedom system with mass proportional damping, which is classically damped, is obtained. Thus, the circular frequencies of the coupled system are the same as those of the undamped one, and the added damping ratio for the modes of the system is

$$\xi_{\text{add},i} = \frac{\alpha}{2\omega_i}, \quad (7)$$

where α and thus the values of c_{di} can be calibrated to achieve a prefixed added damping ratio in correspondence of the first mode of the bare frame.

In the case of the rocking tower, a simplified expression for the damper design can be obtained by assuming infinitely

rigid bracings. Under this assumption, the system acts as a single-degree of freedom, the displacement shape is linear along the building height and controlled by the base rotation ψ , that is, $\mathbf{u} = \psi \mathbf{h}$, where $\mathbf{h} = [h_1, h_2, \dots, h_7, b/2, b/2]^T$ is the vector collecting the floor heights and half of the external bracing frame width b . The corresponding circular vibration frequency and added damping ratio due to the dampers located at the tower base are

$$\omega^2 = \frac{\boldsymbol{\varphi}^T \mathbf{K} \boldsymbol{\varphi}}{\boldsymbol{\varphi}^T \mathbf{M} \boldsymbol{\varphi}} = \frac{\mathbf{h}^T \mathbf{K} \mathbf{h}}{\mathbf{h}^T \mathbf{M} \mathbf{h}} \quad (8)$$

$$\xi_{\text{add}} = \frac{c_d N_d b^2 / 4}{2\omega \mathbf{h}^T \mathbf{M} \mathbf{h}},$$

where c_d is the viscous constant of the N_d dampers located at the tower base. As previously, the value of c_d can be calibrated to achieve a prefixed value of the added damping ratio for the system.

2.2. Stochastic Formulation of the Seismic Problem. The problem can be solved in the frequency-domain, rather than in the time-domain [32]. It is noteworthy that resorting to the frequency-domain has the advantage of allowing for a condensed description of the seismic problem, in terms of the active degrees of freedom only. Moreover, it permits to conveniently estimate the response to the uncertain input by exploiting already available stochastic dynamics techniques.

By denoting with $\bar{\mathbf{x}}$ and $\bar{\mathbf{y}}$ the Fourier transforms of the vectors collecting, respectively, the active degrees of freedom and internal degrees of freedom and with \bar{a}_g the transformed external scalar loading function, representative of the seismic base acceleration, the differential system of (2) can be rewritten as an algebraic system:

$$\left[\begin{array}{c|c} -\omega^2 \mathbf{M}_{xx} + \mathbf{H}_{xx} & \mathbf{H}_{xy} \\ \hline \mathbf{H}_{yx} & \mathbf{H}_{yy} \end{array} \right] \begin{bmatrix} \bar{\mathbf{x}} \\ \bar{\mathbf{y}} \end{bmatrix} = \begin{bmatrix} -\mathbf{M}_{xx} \mathbf{p}_x \\ \mathbf{0} \end{bmatrix} \bar{a}_g, \quad (9)$$

where $\mathbf{H}_{\alpha\beta} = i\omega \mathbf{C}_{\alpha\beta} + \mathbf{K}_{\alpha\beta}$, for $\alpha, \beta = x, y$, and ω is the circular frequency.

Based on (9), the internal displacements can be expressed in function of $\bar{\mathbf{x}}$ as

$$\bar{\mathbf{y}} = -\mathbf{H}_{yy}^{-1} \mathbf{H}_{yx} \bar{\mathbf{x}}. \quad (10)$$

After substituting (10) into (9) and rearranging, the following condensed problem is obtained, where the active displacements can be directly related to the base motion through the expression:

$$\bar{\mathbf{x}} = \mathbf{H}(\omega) \bar{a}_g, \quad (11)$$

where $\mathbf{H}(\omega) = -\mathbf{M}_{xx}[-\omega^2 \mathbf{M}_{xx} + \mathbf{H}_{xx} - \mathbf{H}_{xy} \mathbf{H}_{yy}^{-1} \mathbf{H}_{yx}]^{-1} \mathbf{p}_x$ is the transfer function vector for the problem.

It is noteworthy that both the external damping solutions can be formally expressed in terms of the condensed problem of (11). Thus, the transfer functions of the two systems can be directly compared one to each other and also to the transfer function of the bare frame in order to shed light on the effects of the different types of retrofit.

Moreover, the transfer functions can be useful to estimate the statistic of the response under a stochastic earthquake input. If both the earthquake input and the response are considered stationary, the Power Spectral Density (PSD) of the output $\Phi_{xx}(\omega)$ can be expressed as follows [29]:

$$\Phi_{xx}(\omega) = \mathbf{H}^*(\omega) \Phi_{a_g a_g}(\omega) \mathbf{H}^T(\omega), \quad (12)$$

where $\Phi_{a_g a_g}(\omega)$ is the PSD of the earthquake input and $\mathbf{H}^*(\omega)$ is the complex conjugate of the transfer function vector.

The variance of the i th floor displacement response x_i can be obtained as

$$\sigma_{x_i}^2 = 2 \int_0^\infty [\Phi_{xx}(\omega)]_{ii} d\omega, \quad (13)$$

where $[\Phi_{xx}(\omega)]_{ii}$ denotes the element of matrix $\Phi_{xx}(\omega)$ in correspondence of row i and column i .

Finally, approximate estimates of the peak values of displacement x_i can be obtained based on the concept of the peak factor η_p [30]. The expected value of η_p , evaluated according to the Davenport formula, is

$$E[\eta_p] = \sqrt{2 \log \left(\frac{\omega_c t_L}{\pi} \right)} + \frac{0.5772}{\sqrt{2 \log (\omega_c t_L / \pi)}}, \quad (14)$$

where $\omega_c = \sigma_{\dot{x}_i} / \sigma_{x_i}$ is the central frequency, that is, the ratio between the standard deviation of the velocity and of the displacement of the response, and t_L is the time interval of observation.

The expected value of the maximum displacement response amplitude is thus given by $x_{i\text{max}} = E[\eta_p] \sigma_{x_i}$. The standard deviation of the velocity response $\sigma_{\dot{x}_i}$ can be found as

$$\sigma_{\dot{x}_i}^2 = 2 \int_0^\infty \omega^2 [\Phi_{xx}(\omega)]_{ii} d\omega. \quad (15)$$

The Fourier transform $\bar{\mathbf{q}}$ of the vector collecting any other response parameter of interest \mathbf{q} (e.g., floor accelerations, base shears) can be related to $\bar{\mathbf{x}}$ through the linear operator $\mathbf{B}(\omega)$. Consequently, the PSD of \mathbf{q} can be obtained as follows:

$$\Phi_{qq}(\omega) = \mathbf{B}(\omega) \Phi_{xx}(\omega) \mathbf{B}^T(\omega). \quad (16)$$

The corresponding peak response value for the i th component of \mathbf{q} can be found by considering in (14) the relevant expression of the central frequency; that is, $\omega_c = \sigma_{\dot{q}_i} / \sigma_{q_i}$.

3. Case Study and Seismic Hazard

The Van Nuys building [26–28] is a 7-storey 3 bay-by-8 bay cast-in-place r.c. moment resisting frame building, with nonductile column detailing, designed in 1965 in compliance to the lateral force requirements of 1964 Los Angeles City Building Code. The structural system consists of perimeter moment resisting frames and interior slab-column frames, as shown by the planar view and the transverse section

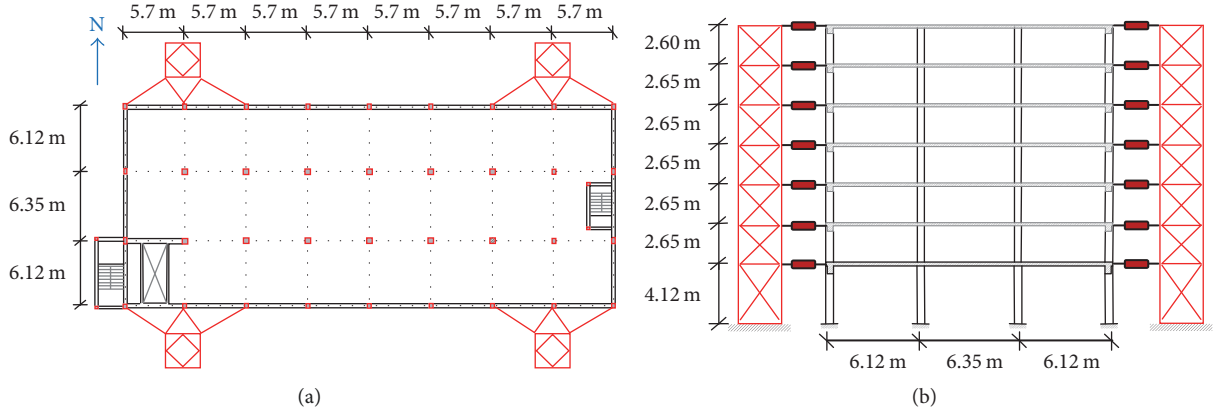


FIGURE 2: Van Nuys Building retrofitted with four fixed-based towers: (a) planar view and (b) transverse N-S section.

(N-S direction) of Figure 2. In the same figure, the four fixed base external braced frames, connected at the floor level to the building by means of FVDs, are illustrated. The rocking braced towers are placed in the same location of the fixed-based frames and also have the same geometrical and mechanical properties.

The dynamic system is described by considering only the motion along the N-S direction. Hereinafter, the bare Van Nuys building is denoted as not-retrofitted “NR” configuration, the building coupled with the fixed base external bracing as “FB” configuration, and the building coupled with the dissipative rocking tower as “RB” configuration. The floors are assumed to be rigid in the horizontal plane and the masses are concentrated at the floor levels so that the vector of active degrees of freedom \mathbf{x} collects the seven floors motions only, for both the two retrofitting configurations. For the purpose of the analysis, a single, equivalent external structure is considered. Thus, the dimension of \mathbf{y} is seven in the case of the FB system, since it collects the horizontal displacements of the dampers at the seven floors of the external braced frame and two in the case of the RB system, since it collects the vertical displacements of the dampers located at the tower base.

The stochastic seismic input considered in all the application examples presented in this paper is a time-modulated Gaussian process whose embedded PSD function is described by the widely used Kanai-Tajimi model modified by the Clough-Penzien filter [31]; that is,

$$S_{CP}(\omega) = S_0 \cdot \frac{\omega_g^4 + 4 \cdot \xi_g^2 \cdot \omega^2 \cdot \omega_g^2}{\left[\omega_g^2 - \omega^2\right]^2 + 4 \cdot \xi_g^2 \cdot \omega^2 \cdot \omega_g^2} \cdot \frac{\omega^4}{\left[\omega_f^2 - \omega^2\right]^2 + 4 \cdot \xi_f^2 \cdot \omega^2 \cdot \omega_f^2} \quad (17)$$

in which S_0 is the amplitude of the bedrock excitation spectrum, modelled as a white noise process; ω_g and ξ_g are the fundamental circular frequency and damping factor of the soil, respectively; ω_f and ξ_f are the fundamental circular frequency and damping factor of the filter, respectively. The values of the soil and filter parameters used hereinafter are

$\omega_g = 15 \text{ rad/s}$, $\xi_g = 0.6$, $\omega_f = 1.5 \text{ rad/s}$, and $\xi_f = 0.6$ [33]. Figure 3 shows the PSD function for $S_0 = 1 \text{ m}^2/\text{s}^3$.

The relation between S_0 and the average peak ground acceleration (PGA) for the stochastic ground motion model employed in this study is obtained by following the procedure outlined in [34]. In particular, a set of 10000 ground motion records is generated by means of the Spectral Representation method [35], by assuming a duration $t_{\max} = 30 \text{ s}$ for the seismic excitation and $S_0 = 1 \text{ m}^2/\text{s}^3$. The mean value of the sample peak ground accelerations is then estimated ($\text{PGA}_{S_0=1} = 34.30 \text{ m/s}^2$), and the value of S_0 corresponding to a prefixed acceleration level PGA is obtained as

$$S_0 = \left(\frac{\text{PGA}}{\text{PGA}_{S_0=1}} \right)^2. \quad (18)$$

For example, a value of $S_0 = 0.0203 \text{ m}^2/\text{s}^3$ is obtained for $\text{PGA} = 0.5g$, where g is the gravity constant.

In order to set up a parametric analysis, a measure of the stiffness of the external system with respect to that of the existing frame is necessary. The global stiffness of the existing frame and that of the external bracings are measured by the parameters K_F and K_T , respectively. These are evaluated by imposing a unit horizontal displacement at the top floor and by evaluating the corresponding base reaction. For the purpose of evaluating K_T , in the case of the rocking tower, a fixed base condition is considered to restrain the motion due to rocking. Thus, the values of K_T are identical for the FB and RB configurations when the external steel braced frames have the same geometrical and mechanical properties. The nondimensional parameter $\kappa = K_T/K_F$ is finally used to quantify the ratio of the external bracing stiffness to the existing frame stiffness, whereas the nondimensional parameter ξ_{add} , already introduced in the previous section, is used to measure the global added damping due to the external system. In particular, for design purposes, the target (design) value of ξ_{add} , evaluated through the expression proposed in the ASCE Standard [36], is considered:

$$\xi_{\text{add}} = \frac{1}{4\pi E_f} \sum_{j=1}^N E_j, \quad (19)$$

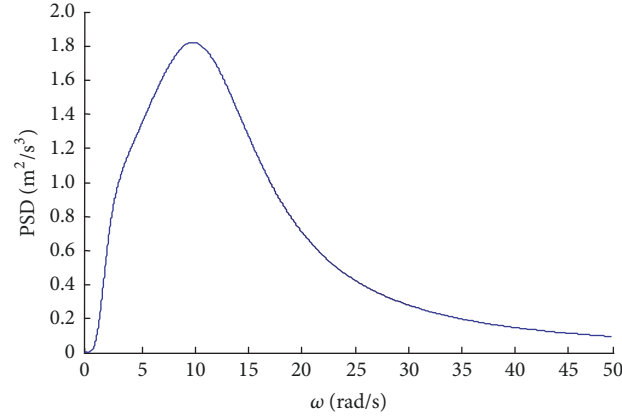


FIGURE 3: PSD of the earthquake input.

TABLE 1: Modal analysis results of the bare building and of the retrofitted building.

Mode	NR			FB			RB		
	T_0 [s]	T_i [s]	ξ_i	T_0 [s]	T_i [s]	ξ_i	T_0 [s]	T_i [s]	ξ_i
(1)	1.204	1.204	0.05	1.204	1.047	0.330	1.168	1.029	0.342
(2)	0.391	0.391	0.05	0.391	0.387	0.143	0.255	0.230	0.131
(3)	0.218	0.218	0.075	0.218	0.217	0.129	0.122	0.118	0.107
(4)	0.138	0.138	0.111	0.138	0.138	0.146	0.078	0.078	0.138
(5)	0.093	0.093	0.161	0.093	0.093	0.185	0.058	0.058	0.182
(6)	0.068	0.068	0.218	0.068	0.068	0.235	0.046	0.046	0.227
(7)	0.056	0.056	0.266	0.056	0.056	0.280	0.040	0.040	0.261

where E_j is the dissipative work done by j th device in one complete vibration cycle at the fundamental frequency of the coupled system and E_f is the relevant maximum strain energy.

The response of the system is initially studied by considering for both the upgrading configurations a reference solution related to the parameters $\kappa = 1$ and $\xi_{\text{add}} = 0.3$, in addition to the inherent damping of the frame equal to 0.05. Once the response of this case is discussed, a parametric analysis is carried out by considering different pairs of stiffness and damping.

3.1. Modal Properties. This section provides an insight into the modal properties of the NR frame and of the FB and RB configurations corresponding to $\kappa = 1$ and $\xi_{\text{add}} = 0.3$, evaluated based on the procedure outlined in Section 2.1. While the NR system has 7 vibration modes only, a total of 7 complex modes and 7 overdamped ones is obtained in the case of the FB system, and 7 complex modes and 2 overdamped ones in the case of the RB system.

Table 1 reports the vibration periods T_i and damping ratios ξ_i of the 7 modes of vibration of interest, which correspond to the 7 active degrees of freedom, for the different systems analyzed. The undamped vibration periods T_{0i} of the three configurations, obtained by neglecting the contribution of the dampers, are also evaluated to estimate the effect of the added damping separately from that of the added stiffness. It is worth observing that the FB configuration exhibits undamped periods that are the same as the NR configuration.

This is because the external frame and the existing one do not interact with each other if the viscous interconnection is disregarded. On the other hand, in the case of the RB configuration, the external rocking tower interacts with the existing one through rigid connections, and this results in a reduction of the modal periods even in the undamped case (from $T_{01} = 1.204$ s to $T_{01} = 1.168$ s). In particular, the relative reduction of the undamped period due to the RB system is small for the first mode, around 3%, but it becomes more significant for the higher modes and it attains the values 35% and 44%, respectively, for the second and third mode.

With reference to the damped dynamic behaviour, it is observed that the first mode damped period of the FB arrangement, $T_1 = 1.047$ s, is 15% lower than the undamped one, $T_{01} = 1.204$ s, and the corresponding damping ratio, $\xi_1 = 0.33$, is close to the design value 0.35 (resulting from the target design value plus the inherent damping). The higher modes are characterized by values of the undamped and damped vibration periods close to each other, and thus similar to those of the NR configurations. The values of the damping ratios are also lower than that of the fundamental mode. The RB configuration is characterized by values of the first mode damped period, $T_1 = 1.029$ s, and of the damping ratio, $\xi_1 = 0.342$, which are very close to those of the FB configuration. The damping ratios of the higher modes are similar to those of the FB and RB systems, whereas the damped periods are lower in the RB case.

This demonstrates again that the RB configuration induces major changes to the dynamic behaviour of the NR

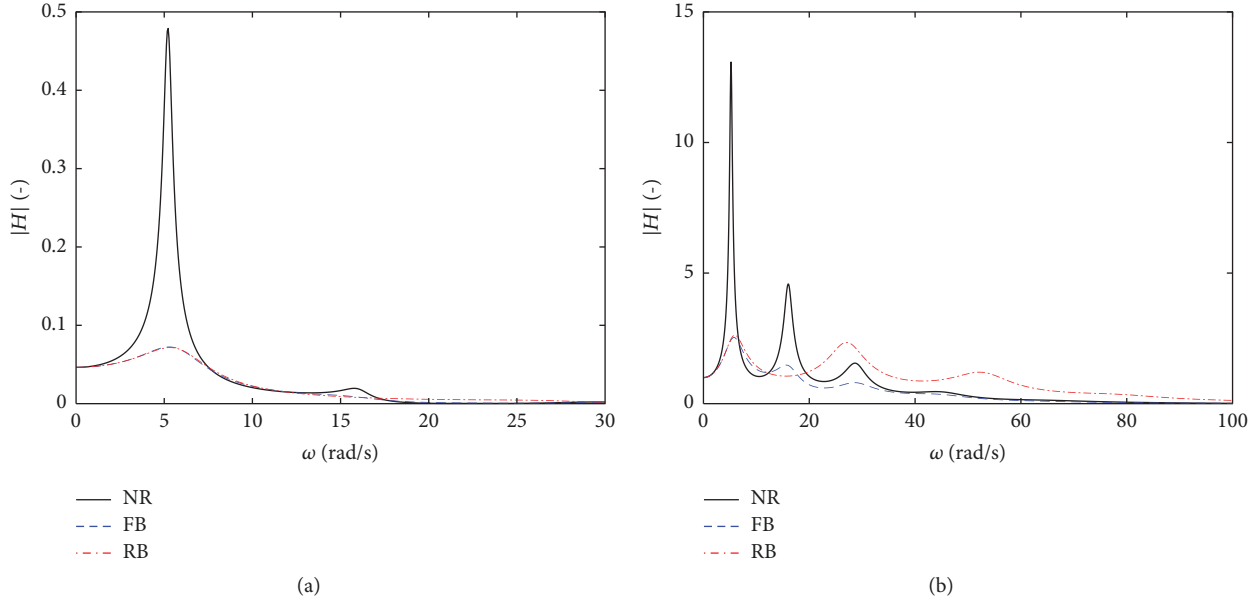


FIGURE 4: FRFs of the NR, FB, and RB systems in terms of (a) top floor displacement; (b) top floor acceleration.

system, compared to the FB system, due to the different nature of the connection between the tower and the frame: viscous in the FB case and rigid in the RB one.

3.2. Frequency Response. This section analyzes the frequency response of the NR frame and of the FB and RB configurations corresponding to $\kappa = 1$ and $\xi_{\text{add}} = 0.3$. This analysis provides a first insight into the modification of the dynamic response in terms of various EDPs of interest due to the retrofit. Figure 4 shows the absolute value of the top floor displacement and absolute acceleration Frequency Response Functions (FRFs).

With reference to the displacement, it can be seen that the response at the top of the NR frame is characterized by a very high peak at the fundamental circular frequency of vibration of the system ($2\pi/T_1 = 5.22$ rad/s), as expected, whereas the influence of higher order modes is negligible. Both the retrofit systems are effective in reducing the response peak, due to the added damping. The shift of the peak is low, because the retrofit systems do not alter significantly the first mode of vibration of the existing frame. The acceleration FRFs have a very different shape compared to the displacement FRFs. This is due to the high influence of the higher order modes, which contribute significantly to the top floor acceleration response, thus resulting in multiple peaks located in correspondence of the circular frequencies of the most relevant vibration modes of the systems, that is, modes 1, 2, and 3. Again, both the retrofit systems allow reducing the peak in correspondence of the first mode of vibration. Moreover, the peaks of the FRF for the FB system are observed in correspondence of the same values of ω of the frame, with the exception of the first peak which is slightly shifted towards higher ω values in the retrofitted configuration. This is the result of the fact that the FB system does not alter significantly the dynamic response of the existing frame, by adding only damping and not stiffness.

On the other hand, the RB system presents a second and third peak in correspondence of higher frequency values compared to the FB and RB systems. This is the consequence of the stiffening effect of the tower, which modifies the period and shape of the higher modes of vibration of the existing frame.

Figure 5 shows the FRF of the base shear of the frame and of the external bracings. It can be observed in Figure 5(a) that the second mode of vibration has a nonnegligible influence on the shear response of the frame, for all the analyzed arrangements. The RB system is more effective in reducing this EDP. On the other hand, the absolute values of the FRF of the external bracings base shear (Figure 5(b)) are always higher for the RB system than for the FB system. Thus, it is interesting to observe the changes of the total base shear due to the retrofit. This is plotted in Figure 6, showing that the addition of the retrofit system to the existing frame results in a reduction of the peak at the fundamental period. However, while the FB system reduces the response also at the other frequencies, the RB system amplifies the response around the value of the circular frequency of 28 rad/s (second mode).

3.3. Stochastic Seismic Response. This section reports and compares the stochastic seismic responses of the NR frame and of the FB and RB configurations corresponding to $\kappa = 1$ and $\xi_{\text{add}} = 0.3$. In particular, Figure 7 shows and compares the PSDs of the EDPs of interest for the different systems analyzed. These PSD are the results of the convolution between the FRFs, illustrated in Figures 4–6, and the PSD of the input, illustrated in Figure 3. It can be observed that the PSD of the input has a peak at the period of 0.5 s. Thus, some resonance effects with the first two modes of vibration of the systems considered are expected. In particular, it is observed in Figure 7 that while the PSD of the top displacement is dominated by the first mode (Figure 7(a)), the PSDs of the other response parameters have multiple peaks. Moreover, as

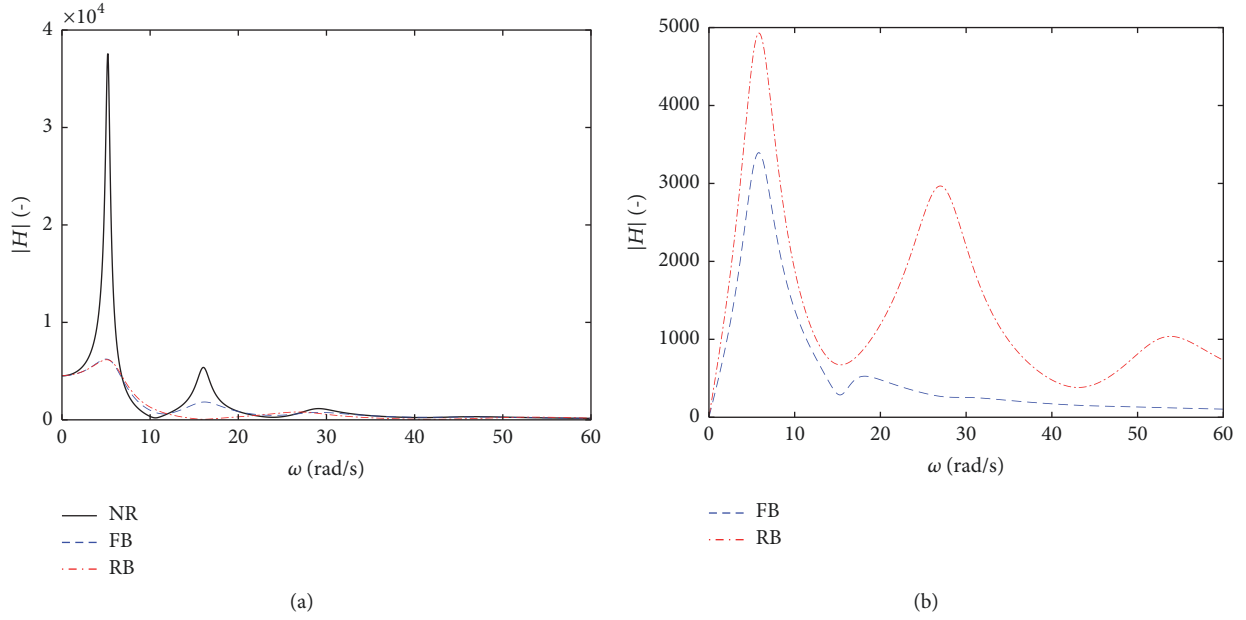


FIGURE 5: FRFs of the NR, FB, and RB systems in terms of (a) frame base shear; (b) external bracing base shear.

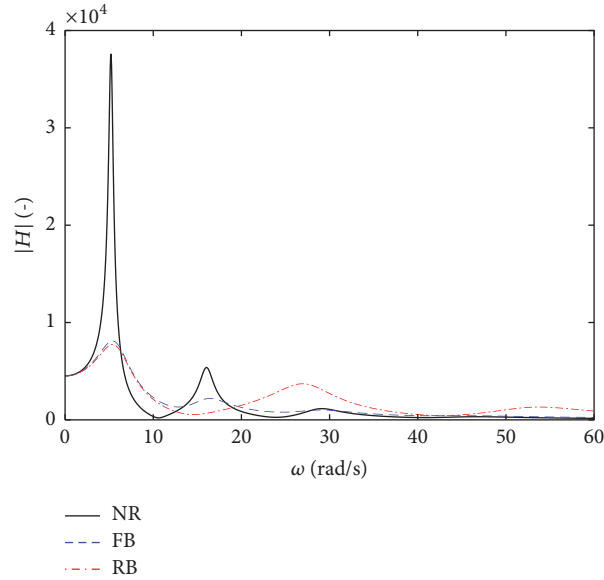


FIGURE 6: FRFs of the NR, FB, and RB systems in terms of total base shear.

in the case of the FRF, the peaks are located approximately in correspondence of the same frequencies in the case of the NR and FB configurations, while in the RB case only the first peak is close to the first peak of the other systems, as a result of the changes that the RB system induces through the added stiffness on the dynamic behaviour of the existing frame. The peak force that a damper has to withstand is an important response parameter, influencing the damper cost together with the damper stroke [37]. Figure 7(f) shows that the PSD of the sum of the damper forces is largely higher for the RB case than for the FB case. This is because the strokes of the dampers in the RB frame are reduced compared to those of the dampers in the FB configuration, and thus higher forces

are required to obtain the same amount of energy dissipation. Obviously, the damper forces coincide with the interaction forces between the frame and the tower in the case of the FB configuration. The cost of the retrofit depends also on these mutual exchange forces between the existing and the external structures, whose PSDs are also plotted in Figures 8(a) and 8(b). It can be seen that the exchange forces are significantly higher for the RB case than for FB case. This is because in the RB case a rigid connection rather than a viscous one is used.

The final part of the current section analyzes the peak values of the responses of interest for the different configurations. Before discussing the results, the accuracy of the method of the peak factor is evaluated comparing the average

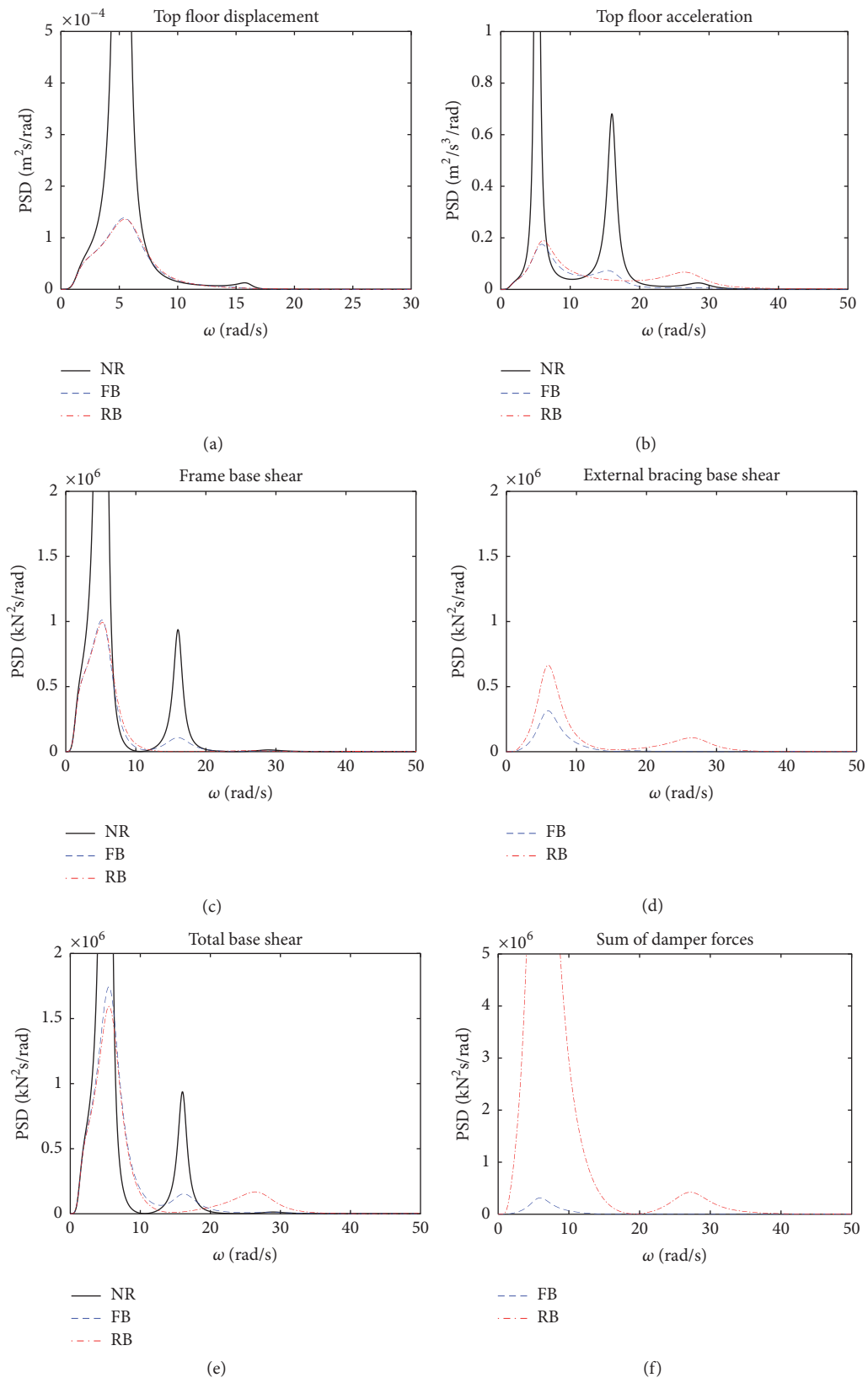


FIGURE 7: PSD of the response parameters of interest for the NR, FB, and RB configurations.

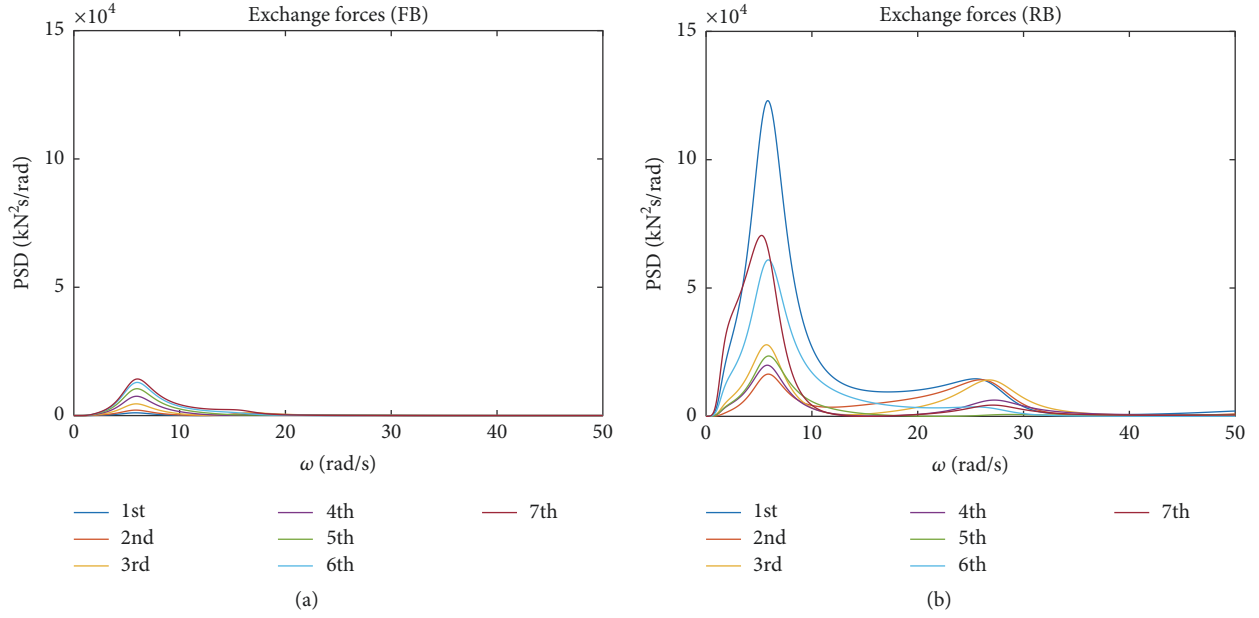


FIGURE 8: PSD of the exchange forces for the FB (a) and RB (b) configurations.

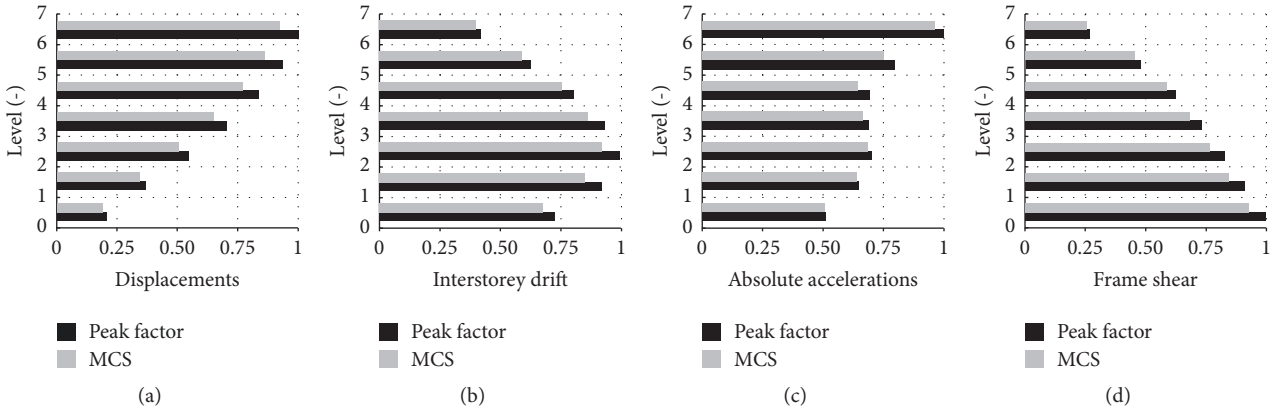


FIGURE 9: Comparison of the response parameters of interest for the NR configuration obtained through the peak factor estimation and through MCS approach.

peak responses of the NR case obtained with $E[\eta_p]$ estimated via (14) against the mean of the maxima resulting from a Monte Carlo Simulation (MCS) approach based on the frequency analysis of the system under 500 of sample seismic inputs.

Figure 9 shows the distribution of the floor displacements, interstorey drifts, absolute accelerations, and shear actions of the NR configuration according to MCS and to the peak factor method. Each response parameter is normalized to have the estimate through the peak factor method equal to one. In particular, Figure 9(a) shows the displacements distribution along the height of the building, which presents a maximum value at the top. The interstorey drifts (IDRs) distribution, reported in Figure 9(b), is not regular and the maximum is attained in correspondence of the third storey. Figure 9(c) shows the absolute accelerations at the different floors, which have S-shaped distribution, highly influenced by higher order

modes, even though the maximum value is observed at the top. Finally, Figure 9(d) illustrates the shear actions resisted by the frame. Using the peak factor results in general in an overestimation of the maxima, with relative errors between 3.7% and 8.2% for all the EDPs of interest. The same technique applied to the analysis of the two retrofit configurations (FB and RB) also leads to a general underestimation of the maxima, but with a maximum relative error lower than 3%. Given the high accuracy of the obtained estimates, the response values reported hereinafter are those obtained via the peak factor method, which is computationally more efficient than MCS.

Figure 10 illustrates and compares the performances of the NR, FB, and RB configurations in terms of peak EDPs values estimated via the peak factor method. For each EDP considered, the peak values are normalized so that they are equal to unit in the NR case. This allows highlighting the benefits of the retrofit in terms of response reduction.

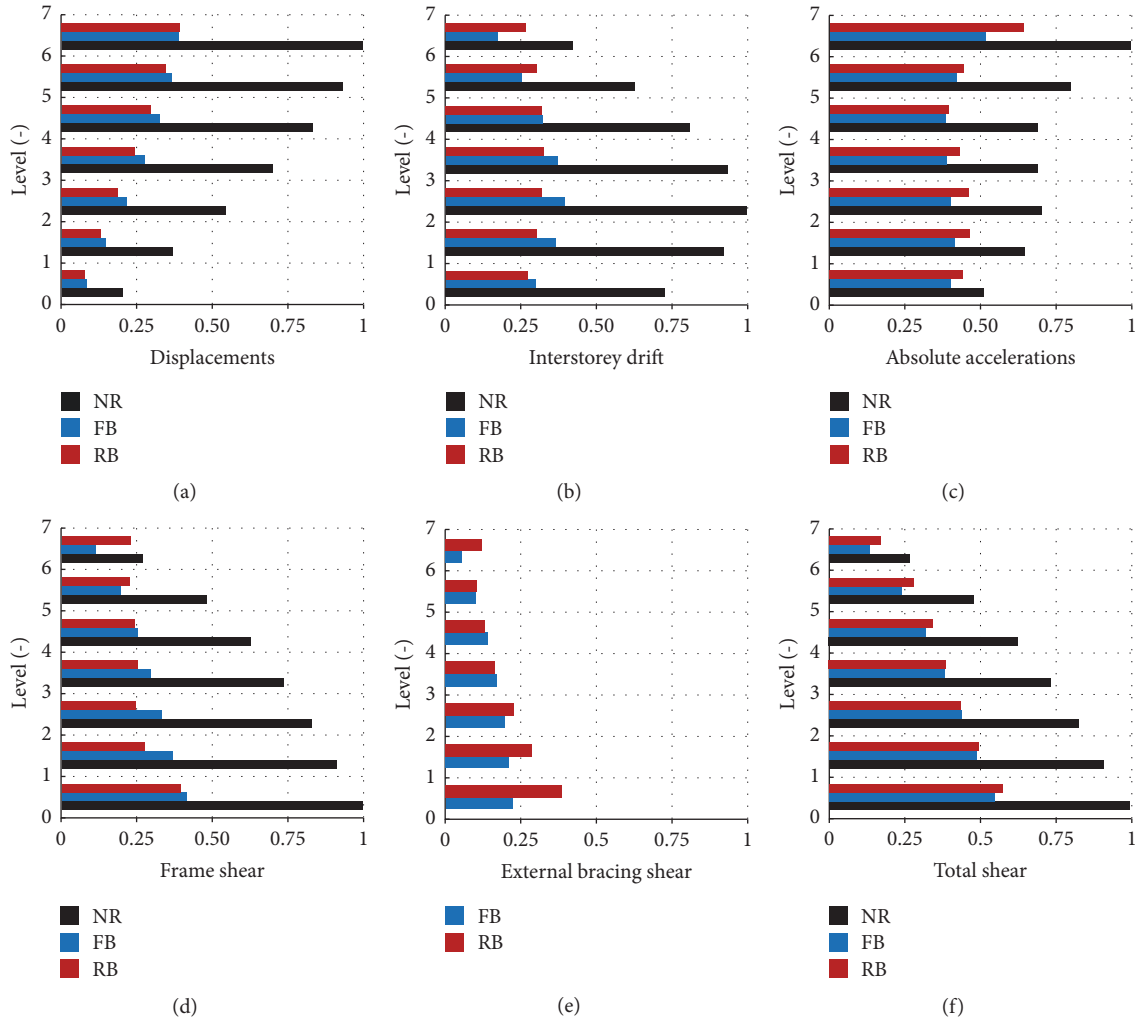


FIGURE 10: Comparison of the seismic performance of the NR, FB, and RB configurations in terms of parameters of interest.

Figure 10(a) illustrates the floor displacements distribution along the height of the building. It can be seen that the deformed shape of the existing frame remains the same after the retrofit in the FB case, whereas it is modified and linearized in the RB case. The relative reduction of the top floor displacements is nearly 61% for both the FB and RB configurations. The reduction values are similar for the two systems because the displacements are controlled by the first mode response, and the added damping ratio for this mode is nearly the same. The drift demand regularization in the case of the RB system can be better visualized in Figure 10(b), showing the interstorey drifts (IDRs) responses. The IDRs are lower in the RB system than in the FB system at the lower storeys and higher at the last two storeys.

Figure 10(c) shows the values of the floor absolute accelerations observed at the various levels of the building for the configurations investigated. The shape of the floor accelerations is not significantly modified after the retrofit, and both the FB and the RB configurations induce a reduction of the maximum absolute acceleration values with respect to the bare frame (NR). A better result in terms of maximum

acceleration reduction is achieved with the FB system. This system allows a maximum reduction of the accelerations of 48% in correspondence of the last floor, while the rocking tower provides a maximum reduction of 36%. This result is of particular importance for the performance evaluation of acceleration-sensitive nonstructural components and may impair the benefits of the retrofit with the rocking system.

As already discussed for the displacements, the addition of the two external dissipative systems results in a reduction of the base shear demand in the frame; in the FB case the reduction is equal to 59%, whereas in the RB case it is equal to 61% (Figure 10(d)). In general, the reduction is different from storey to storey in the FB configuration, with higher reduction at the higher storeys, while it is nearly the same at the various storeys in the RB configuration. The RB configuration also provides a more regular distribution of the shear at the different storeys compared to the other configurations. Figure 10(e) shows the values of the shear action resisted by the external structures of the retrofit configurations, normalized with respect to the frame shear of the bare building. The RB case results in higher values at

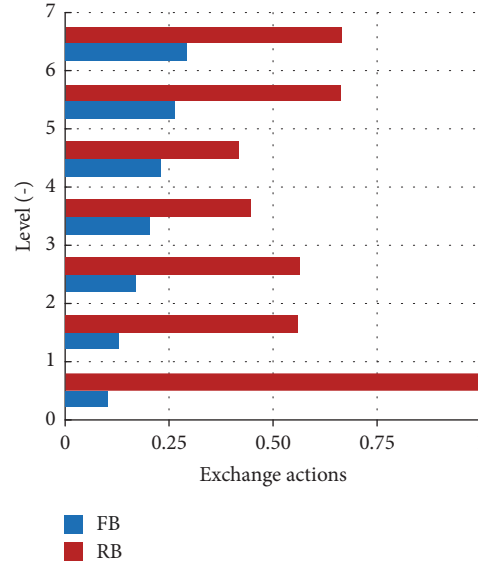


FIGURE 11: Exchange actions for the FB and RB configurations.

almost all the elevations, especially at lower storeys. Finally, Figure 10(f) illustrates the total storey shear. Again, the two retrofit systems exhibit similar performances in terms of base shear reduction, which is equal to 45% and 42%, respectively, in the FB and RB configurations.

Figure 11 illustrates the distribution of exchange actions for the two retrofit cases. In the FB system, where a damped connection system is used, these forces coincide with the internal axial actions in the FVDs, whose trend has already been discussed previously. In the RB configuration, the connection system is rigid, and the interaction forces are elastic and significantly higher than those of the FB case.

3.4. Parametric Study. In order to understand how the stiffness and added damping of the external FB and RB frames influence the seismic performance of the coupled system, a parametric study is carried out by varying the nondimensional parameters κ and ξ_{add} representing, respectively, the external structures-to-existing frame stiffness and the added design damping ratio and by evaluating the corresponding changes in the seismic response. Three values of the parameters κ and ξ_{add} are taken into account, that is, $\kappa = 0.25, 0.5, 1$ and $\xi_{add} = 0.1, 0.2, 0.3$.

Figure 12 shows the results obtained for the two retrofit configurations in terms of the following monitored EDPs: the top floor displacement and absolute acceleration, the third floor interstorey-drift, the base shear of the frame and of the external structure, and the total base shear. The results are normalized such that the EDP values are unit in the case of the NR frame. With regard to the top floor displacement response (Figure 12(a)), it can be observed in general that both the FB and RB cases yield similar results, with a relative reduction between 38% and 61% in the FB system and a reduction between 40% and 61% in the RB system, with respect to the NR case. Higher values of the added damping result in a higher reduction of the displacement demand, as expected.

Although the best performance is achieved for $\kappa = 1$ and $\xi_{add} = 0.3$ in both the configurations, a good response reduction is obtained also for $\kappa = 0.5$ and $\xi_{add} = 0.3$, while for $\kappa = 0.25$ the external structure is too flexible to resist the motion of the existing structure and activate the dampers. In fact, if ξ_{add} is low, the external structure does not need to be very stiff to activate the dampers. On the other hand, if ξ_{add} is high, a stiff external frame is required for the dampers to be effective.

Figure 12(b) shows the third floor interstorey drifts for the different configurations and parameter combinations. The relative reduction achieved is in the range of 38% to 60% in the FB configuration, and in the range of 45%–68% in the RB configuration. As already observed for the displacements, the best result are achieved for $\kappa = 1$ and $\xi_{add} = 0.3$, and the case $\kappa = 0.25$ is characterized by a reduced efficiency with respect to the other ones.

Figure 12(c) shows the results in terms of top floor absolute acceleration. The FB case provides the best result for any combination of κ and ξ_{add} . The relative reduction of this EDP for this case is between 28% and 48%, while it is between 18% and 37% in the RB case. Increasing the damping results in a reduction of the accelerations in the FB case but can increase the accelerations in the RB case for some values of κ and ξ_{add} . In fact, in the RB configuration the highest value of ξ_{add} yields also the highest acceleration demand for both $\kappa = 0.25$ and $\kappa = 0.5$, and this could affect the effectiveness of such retrofit scheme, when the protection of acceleration-sensitive components is a design objective. For $\kappa = 1$, similar acceleration reductions are achieved for $\xi_{add} = 0.2$ and $\xi_{add} = 0.3$.

Figures 12(d)–12(f) describe the response in terms of frame base shear, external bracing base shear, and total base shear. Figure 12(d) shows that the relative reduction of the frame base shear is between 37% and 59% in the FB case, and between 38% and 61% in the RB case. Moreover, in the RB case the frame base shear reduction is not significantly affected by variations of κ , particularly for low damping

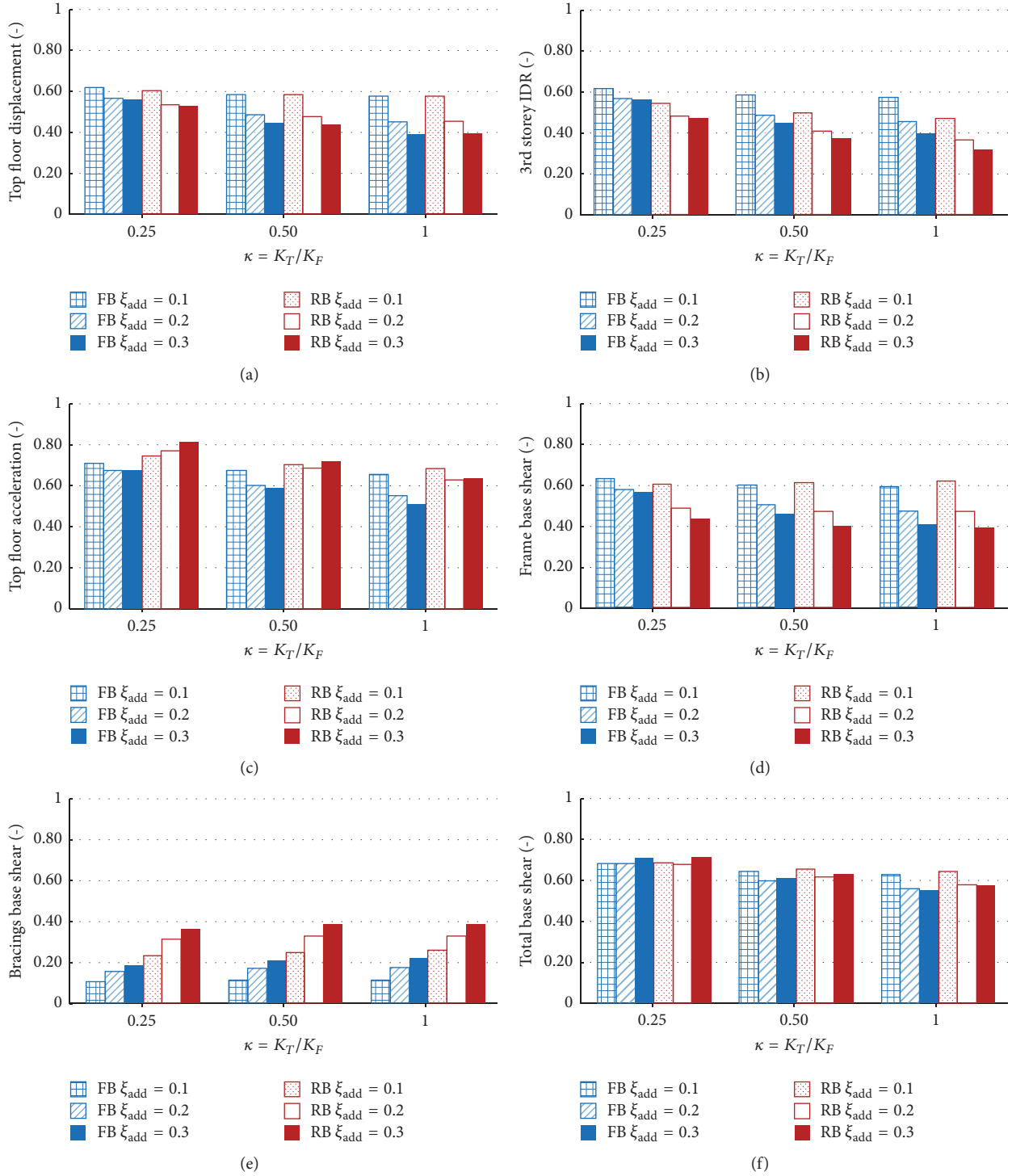


FIGURE 12: Results of the parametric analysis for the FB and RB configurations in terms of different EDPs of interest.

values. On the other hand, the retrofit effectiveness of the FB configuration reduces significantly by considering external frames with $\kappa = 0.25$ rather than $\kappa = 0.5$ or $\kappa = 1$. Figure 12(e) describes the base shear resisted by the external structures. This parameter is more sensible to the added damping rather than to the stiffness ratio. Generally, higher values of κ and ξ_{add} result in higher values of the bracing base shear. The

values of the base shear of the external structures normalized with respect to that of the bare frame are comprised between 11% and 22% in the FB case, while they are between 23% and 39% in the RB case. Finally, from Figure 12(f) it is evident that the total base shear reduction provided by the FB and RB case is nearly the same, no matter what values of the stiffness ratio or of the added damping are considered, with a relative

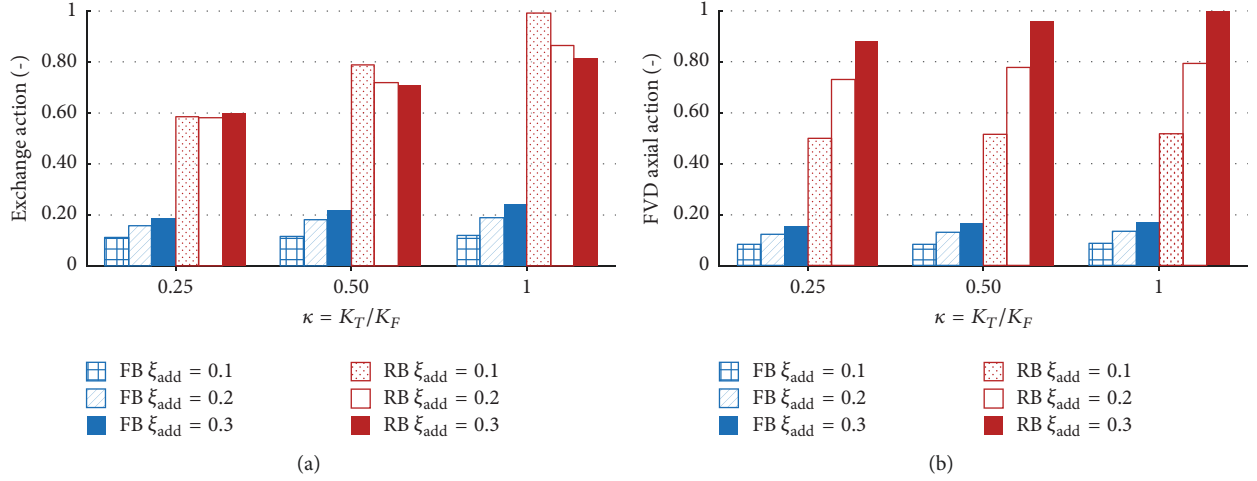


FIGURE 13: Results of the parametric analysis for the FB and RB configurations in terms of (a) exchange forces between one external frame and the existing frame and (b) sum of the forces of the FVDs.

reduction of the shear resisted by the bare frame between 32% and 45% for the FB configuration and between 29% and 42% for the RB case, with respect to the NR frame.

Figure 13(a) illustrates the values of the maximum exchange forces between the external frames and the existing structure. In the case of the FB configuration, these correspond to the exchange forces at the top floor, whereas in the RB configuration these correspond to the exchange forces at the first floor (see Figure 11). The values for the different combinations of κ and ξ_{add} are normalized so that the exchange forces in the case of $\kappa = 1$ and $\xi_{add} = 0.1$ are equal to unit in the RB configuration, which is in general characterized by higher values compared to the FB configuration. It can be observed that, in the FB system, increasing κ does not affect significantly the force demand, whereas increasing ξ_{add} yields an increase of forces. On the other hand, in the RB configuration, increasing κ results in an increase of forces, and increasing ξ_{add} reduces the forces for $\kappa = 0.5$ and $\kappa = 1$. Figure 13(b) shows the maximum values of the sum of the damper forces for the two retrofit configurations. In general, these forces increase by increasing ξ_{add} , whereas they do not increase significantly by increasing κ . Higher values are observed in the RB system for all the combination $\kappa - \xi_{add}$ analyzed.

4. Conclusions

In this paper, two alternative arrangements of external passive retrofitting systems are analyzed, each one characterized by a different kinematic behaviour. The former (FB configuration) consists of an external fixed base steel braced frame connected to the existing one by means of dampers placed horizontally at the floor levels. The latter system (RB configuration) is an innovative one, based on coupling the building with a “dissipative tower,” which is a steel braced frame, hinged at the foundation level, and activating the dampers through its rocking motion. The two systems are nonclassically damped and the analysis of the performance under the uncertain earthquake input is carried out by

means of a general formulation involving stochastic dynamics concepts, which allows efficiently estimating the peak values of the responses of interest and thus carrying out parametric studies for different values of the stiffness and added damping of the external structures. In particular, the FB and RB retrofit configurations are synthetically described by the parameter κ , measuring the ratio between the global stiffness of the external frames to that of the existing frame, and by the external frames design added damping ratio ξ_{add} .

First, the case corresponding to $\kappa = 1$ and $\xi_{add} = 0.3$ is analyzed in detail. The results show that the two retrofit configurations are characterized by similar performances in terms of reduction of the top displacement, interstorey drifts and total shear demand with respect to the nonretrofitted (NR) case. The RB system yields the best distribution of interstorey drifts, due to a linearization of the displacements distribution. On the other hand, this solution is characterized by higher external bracing shear actions and higher absolute floor accelerations, with respect to the FB system. The peak values of the internal actions are lower in the FB system, thanks to the viscous interconnection which does not induce significant changes in the modal shapes of the existing frame. The forces exchanged between the external bracings and the existing frame at the links placed at storey levels are significantly higher in the RB case with respect to forces observed in the interconnecting dampers in the FB case.

In the following part of the paper, a parametric analysis is carried out by considering different values of κ and ξ_{add} for the two retrofitting systems and observing the changes in the response parameters usually considered in design practice. The cases corresponding to $\kappa = 0.5$ and $\kappa = 1$ provide nearly the same performance in terms of the response parameters considered, with the exception of the exchange forces in the RB configuration, which increase significantly by passing from $\kappa = 0.5$ to $\kappa = 1$. This result has significant cost implications, because lower κ values correspond to smaller steel profiles.

The FB system provides the best performance in terms of reduction of absolute accelerations of the top floor compared

to the RB system for all the nondimensional parameter combinations. Moreover, the top floor absolute acceleration generally increases by increasing the added damping in the RB case. The total base shear in the two retrofit configurations is nearly the same for all the values of κ and ξ_{add} considered. The existing frame base shear and the external bracings shear, respectively, decrease and increase by increasing ξ_{add} , while they are less sensitive to variations of κ . Finally the RB configuration provides always higher values of both exchange forces and axial actions in the FVDs, with respect to the FB case, for all the values of κ and ξ_{add} considered.

Conflicts of Interest

The authors declare that there are no conflicts of interest regarding the publication of this paper.

Acknowledgments

The study reported in this paper was partially supported by the Italian Department of Civil Protection within the Reluis-DPC Projects 2017. The authors gratefully acknowledge this financial support.

References

- [1] M. D. Symans and M. C. Constantinou, "Passive fluid viscous damping systems for seismic energy dissipation," *ISOT Journal of Earthquake Technology*, vol. 35, no. 4, pp. 185–206, 1998.
- [2] C. Christopoulos and A. Filiatrault, *Principles of Passive Supplemental Damping and Seismic Isolation*, IUSS Press, Pavia, Italy, 2006.
- [3] L. Ragni, L. Dezi, A. Dall'Asta, and G. Leoni, "HDR devices for the seismic protection of frame structures: Experimental results and numerical simulations," *Earthquake Engineering & Structural Dynamics*, vol. 38, no. 10, pp. 1199–1217, 2009.
- [4] J. K. Whittle, M. S. Williams, T. L. Karavasilis, and A. Blakeborough, "A comparison of viscous damper placement methods for improving seismic building design," *Journal of Earthquake Engineering*, vol. 16, no. 4, pp. 540–560, 2012.
- [5] A. Di Cesare, F. C. Ponzo, D. Nigro, M. Dolce, and C. Moroni, "Experimental and numerical behaviour of hysteretic and visco-recentring energy dissipating bracing systems," *Bulletin of Earthquake Engineering*, vol. 10, no. 5, pp. 1585–1607, 2012.
- [6] J.-S. Hwang, W.-C. Lin, and N.-J. Wu, "Comparison of distribution methods for viscous damping coefficients to buildings," *Structure and Infrastructure Engineering*, vol. 9, no. 1, pp. 28–41, 2013.
- [7] O. Lavan and M. Avishur, "Seismic behavior of viscously damped yielding frames under structural and damping uncertainties," *Bulletin of Earthquake Engineering*, vol. 11, no. 6, pp. 2309–2332, 2013.
- [8] A. Dall'Asta, E. Tubaldi, and L. Ragni, "Influence of the nonlinear behavior of viscous dampers on the seismic demand hazard of building frames," *Earthquake Engineering & Structural Dynamics*, vol. 45, no. 1, pp. 149–169, 2016.
- [9] A. Dall'Asta, F. Scozzese, L. Ragni, and E. Tubaldi, "Effect of the damper property variability on the seismic reliability of linear systems equipped with viscous dampers," *Bulletin of Earthquake Engineering*, vol. 15, no. 11, pp. 5025–5053, 2017.
- [10] F. Freddi, E. Tubaldi, L. Ragni, and A. Dall'Asta, "Probabilistic performance assessment of low-ductility reinforced concrete frames retrofitted with dissipative braces," *Earthquake Engineering & Structural Dynamics*, vol. 42, no. 7, pp. 993–1011, 2013.
- [11] C. Passoni, A. Belleri, A. Marini, and P. Riva, "Existing structures connected with dampers: state of the art and future developments," in *Proceedings of the 2nd European Conference on Earthquake Engineering and Seismology*, pp. 25–29, Istanbul, Turkey, 2014.
- [12] T. Trombetti and S. Silvestri, "Novel schemes for inserting seismic dampers in shear-type systems based upon the mass proportional component of the Rayleigh damping matrix," *Journal of Sound and Vibration*, vol. 302, no. 3, pp. 486–526, 2007.
- [13] O. Lavan and D. Abecassis, "Seismic behavior and design of wall-EDD-frame systems," *Frontiers in Built Environment*, vol. 1, 2015.
- [14] Z. Yang, Y. L. Xu, and X. L. Lu, "Experimental seismic study of adjacent buildings with fluid dampers," *Journal of Structural Engineering*, vol. 129, no. 2, pp. 197–205, 2003.
- [15] V. Gattulli, F. Potenza, and M. Lepidi, "Damping performance of two simple oscillators coupled by a visco-elastic connection," *Journal of Sound and Vibration*, vol. 332, no. 26, pp. 6934–6948, 2013.
- [16] E. Tubaldi, M. Barbato, and A. Dall'Asta, "Performance-based seismic risk assessment for buildings equipped with linear and nonlinear viscous dampers," *Engineering Structures*, vol. 78, pp. 90–99, 2014.
- [17] E. Tubaldi, M. Barbato, and A. Dall'Asta, "Efficient approach for the reliability-based design of linear damping devices for seismic protection of buildings," *ASCE-ASME Journal of Risk and Uncertainty in Engineering Systems, Part A: Civil Engineering, Special Issue on Stochastic Dynamics and Reliability Analysis of Structural and Mechanical Systems Subject to Environmental Excitations*, vol. 2, no. 2, 2016.
- [18] E. Tubaldi, "Dynamic behavior of adjacent buildings connected by linear viscous/viscoelastic dampers," *Structural Control and Health Monitoring*, 2015.
- [19] L. Gioiella, E. Tubaldi, F. Gara, and A. Dall'Asta, "Modal properties and seismic response of existing building retrofitted by external bracings with viscous dampers," in *Proceedings of the 7th European Congress on Computational Methods in Applied Sciences and Engineering, ECCOMAS Congress 2016*, pp. 5156–5171, Crete Island, Greece, June 2016.
- [20] N. Makris and M. Aghagholizadeh, "The dynamics of an elastic structure coupled with a rocking wall," *Earthquake Engineering & Structural Dynamics*, vol. 46, no. 6, pp. 945–962, 2017.
- [21] Z. Qu, A. Wada, S. Motoyui, H. Sakata, and S. Kishiki, "Pin-supported walls for enhancing the seismic performance of building structures," *Earthquake Engineering & Structural Dynamics*, vol. 41, no. 14, pp. 2075–2091, 2012.
- [22] D. Wu and X. L. Lu, "Structural performance evaluation of a new energy-dissipation and light-weight rocking frame by numerical analysis and experiment," in *Proceedings of the 10th Pacific Conference on Earthquake Engineering Building and Earthquake-Resilient*, Sydney, Australia, November 2015.
- [23] D. Roia, F. Gara, A. Balducci, and L. Dezi, "Dynamic tests on an existing r.c. school building retrofitted with "dissipative towers"," in *Proceedings of the 11th International Conference on Vibration Problems*, Lisbon, Portugal, September 2013.
- [24] D. Roia, F. Gara, A. Balducci, and L. Dezi, "Ambient vibration tests on a reinforced concrete school building before and after

- retrofitting works with external steel “dissipative towers,” in *Proceedings of the 9th International Conference on Structural Dynamics, EURODYN 2014*, pp. 2509–2516, Porto, Portugal, July 2014.
- [25] A. Balducci, Dissipative Towers. Application n. EP2010074723820100831, WO2010EP62748 20100831, International and European classification E04H9/02 – Italian concession n 0001395591, 2005.
 - [26] J. Blume, “Holiday Inn,” in *San Fernando Earthquake of February 9, 1971*, vol. I, part A, chapter 29, U.S. Department of Commerce, National Oceanic and Atmospheric Administration, Washington, DC, USA, 1973.
 - [27] K. A. Porter, J. L. Beck, and R. V. Shaikhutdinov, “Investigation of sensitivity of building loss estimates to major uncertain variables for the Van Nuys testbed,” PEER Report 2002/2003 4, College of Engineering, University of California, 2002.
 - [28] H. Krawinkler, “Van Nuys Hotel building testbed report: exercising seismic performance assessment,” PEER Report 2005/2011, Department of Civil and Environmental Engineering, Stanford University, October 2005.
 - [29] L. D. Lutes and S. Sarkani, *Random vibrations: Analysis of Structural and Mechanical Systems*, Elsevier Butterworth-Heinemann, Burlington, 2004.
 - [30] A. Preumont, *Twelve Lectures on Structural Dynamics*, vol. 198, Springer, 2013.
 - [31] R. W. Clough, J. Penzien, and D. S. Griffin Computers and Structures Inc., Berkeley, 2003.
 - [32] L. Gioiella, E. Tubaldi, F. Gara, L. Dezi, and A. Dall’Asta, “Analysis and comparison of two different configurations of external dissipative systems,” in *Proceedings of the 10th International Conference on Structural Dynamics, EURODYN 2017*, pp. 164–169, September 2017.
 - [33] A. D. Kiureghian and A. Neuenhofer, “Response spectrum method for multi-support seismic excitations,” *Earthquake Engineering & Structural Dynamics*, vol. 21, no. 8, pp. 713–740, 1992.
 - [34] E. Tubaldi, M. Barbato, and S. Ghazizadeh, “A probabilistic performance-based risk assessment approach for seismic pounding with efficient application to linear systems,” *Structural Safety*, vol. 36–37, pp. 14–22, 2012.
 - [35] M. Shinozuka and G. Deodatis, “Simulation of stochastic processes by spectral representation,” *Applied Mechanics Reviews*, vol. 44, no. 4, pp. 191–204, 1991.
 - [36] ASCE Standard ASCE/SEI 41-13, *Seismic Evaluation and Retrofit of Existing Buildings*, American Society of Civil Engineers, Reston, VA, USA, 2014.
 - [37] D. Altieri, E. Tubaldi, M. de Angelis, E. Patelli, and A. Dall’Asta, “Reliability-based optimal design of nonlinear viscous dampers for the seismic protection of structural systems,” *Bulletin of Earthquake Engineering*, pp. 1–20, 2017.

